Nanoscale



PAPER

View Article Online



Cite this: Nanoscale, 2022, 14, 8677

Putting together the puzzle of ion transfer in single-digit carbon nanotubes: mean-field meets ab initio†

Vadim Neklyudov Da and Viatcheslav Freger ** *a,b,c

Nature employs channel proteins to selectively pass water across cell membranes, which inspires the search for bio-mimetic analogues. Carbon nanotube porins (CNTPs) are intriguing mimics of water channels, yet ion transport in CNTPs still poses questions. As an alternative to continuum models, here we present a molecular mean-field model that transparently describes ion coupling, yet unlike continuum models, computes *ab initio* all required thermodynamic quantities for the KCl salt and H⁺ and OH⁻ ions present in water. Starting from water transfer, the model considers the transfer of free ions, along with ion-pair formation as a proxy of non-mean-field ion-ion interactions. High affinity to hydroxide, suggested by experiments, making it a dominant charge carrier in CNTPs, is revealed as an exceptionally favorable transfer of KOH pairs. Nevertheless, free ions, coexisting with less mobile ion-pairs, apparently control ion transport. The model well explains the observed effects of salt concentration and pH on conductivity, transport numbers, anion permeation and its activation energies, and current rectification. The proposed approach is extendable to other sub-nanochannels and helps design novel osmotic materials and devices.

Received 8th December 2021, Accepted 30th April 2022 DOI: 10.1039/d1nr08073c

rsc.li/nanoscale

The world is facing water stress, which is predicted to increase and spread to areas not experiencing the shortage of fresh water today. Production of fresh water *via* desalination of seawater, brackish water, and wastewater is a viable solution, yet currently used membrane desalination technology still leaves room for improvement and selectivity-tailoring. This motivates research that looks into alternative materials with improved water–salt and ion–ion selectivity. Natural membrane proteins aquaporins efficiently separate water from ions by forcing it through a short and narrow channel in a single-file arrangement at rates exceeding 109 water molecules per second with nearly ideal water–ion selectivity. Intriguingly, while the use of degradable aquaporins might be impractical, stable nanomaterials, such as atomically thin nanoporous nanosheets or narrow nanotubes, 100 that can mimic transport in aquapor-

Single-digit carbon nanotube porins (CNTPs) share many unique features of aquaporins and demonstrate a water-salt selectivity of 10⁵, commensurate with the selectivity of polyamide desalination membranes, the industrial benchmark. 13-15 Numerous theoretical and experimental studies indicate that, due to wall roughness smaller than the de Broglie length, water transport in CNTPs narrower than about 1.5 nm and similarly narrow-graphene slits occurs in a scatterless manner, at rates greatly exceeding hydrodynamic predictions^{9,30,31} and even faster than water permeation in aquaporins. 22,25 However, while there is an overall consensus regarding water transport in narrow CNTs, the physical mechanisms behind ion rejection still pose many questions. For instance, it has been long believed that negative carboxylic charges at CNTP rims control salt rejection, 32-34 yet recent data on pH dependence of anion permeation downplayed this mechanism. Adsorption of OH ions was proposed as an alternative charging mechanism in CNTs and a number of continuum-type nanofluidic models, solving the Poisson-Boltzmann and Navier-Stokes equations employed this and other ad hoc assumptions to describe transport, charge formation and conduction in narrow and wide CNTPs and rationalize the observed trends. 27,35-41 In parallel, important insights into the transport of ions at the molecular level were obtained using molecular dynamics (MD)⁴²⁻⁴⁵ and *ab initio* computations. 13,46

ins offer an exciting next-generation alternative to currently used polymeric membranes. 11,12

^aWolfson Department of Chemical Engineering, Technion – IIT, Haifa 32000, Israel. E-mail: vfreger@technion.ac.il; Tel: +972 (0) 4 829 2933

^bRussel Berrie Nanotechnology Institute, Technion – IIT, Haifa 32000, Israel ^cGrand Technion Energy Program, Technion – IIT, Haifa 32000, Israel

[†] Electronic supplementary information (ESI) available: Additional details of quantum-chemical calculations, benchmarking of hydration energies and interaction with benzene, derivation of the relation for CNTP conductance, calculation of the limiting rate of salt permeation, transfer parameters for ions and ion pairs obtained from *ab initio* calculations, compiled literature data of ionic mobilities in CNTPs, fitting of transfer excess Gibbs energies to experimental data on conductivity and anion permeation in vesicles, and interpolation of the water transfer energies. See DOI: https://doi.org/10.1039/d1nr08073c

The data on ion permeation in CNTPs have been mainly obtained from two types of measurements: (a) ion permeation from stop-flow experiments with CNTP-loaded vesicles and (b) conductance or current-voltage (I-V) measurements for CNTPs connecting two solutions across a nanopore. These experiments yielded absolute values of permeabilities to different ions and salts, conductivity and water-salt selectivity for various types of CNTPs and longer tubes. They also determined the trends that describe the dependence of transport properties on salt concentration and pH, as well as temperature dependence, from which appropriate activation energies could be derived. These trends are often highly characteristic and may serve as fingerprints of physical mechanisms. The data, combined with simulations, e.g., using classical MD⁴²⁻⁴⁵ and ab initio computations 13,46 have significantly advanced the understanding of ion transport in CNTPs, yet a full and physically consistent picture unifying different experimental findings is still missing.

Here, we develop a systematic molecular picture that transparently describes ion transfer in CNTPs in a hybrid approach. As an alternative to common continuum nanofluidic models, the present model similarly accounts for ion coupling using analytical mean-field relations, yet employs ab initio computations rather than classical electrokinetic relations to evaluate quantities pertaining to ion transfer in narrow channels of molecular width. Since KCl has been the salt most often used in experimental studies, we focus on K⁺ and Cl⁻ ions, adding to the picture the OH and H ions inherently present in water. We focus on (6,6) CNTPs of diameter 0.8 nm, used in most experiments as benchmark sub-nanometer ("singledigit") channels but, in order to clarify the effect of CNTP diameter and water arrangement, the results with narrower (5,5) channels were compared, in which a single-file arrangement is preserved. Importantly, we also consider the effect of the medium surrounding CNTPs that was shown to strongly affect ion transfer from a solution to CNTPs. 47 We first incorporate the computed thermodynamic values in a model considering only free ions, retaining their full translational freedom, which is shown to agree semi-quantitatively with most experimental results. Subsequently, we add to the picture the formation of ion pairs, as a proxy of non-mean-field ion-ion-CNTP interactions, which removes most remaining inconsistencies. The resulting physical picture rationalizes most results on ion permeation, selectivity, conductance, and current rectification in CNTPs reported so far.

Internal arrangement of water and ion hydration: not necessarily a single file

The narrowest experimentally studied CNTPs, showing the largest water-ion selectivity, have been the (6,6) nanotubes. Classical MD simulations suggested that water in (6,6) tubes forms a single file, similar to (5,5) nanotubes, believed to be the narrowest ones that allow water and ion transport. 16,40,48,49 Ions in (5,5) tubes are then solvated by only two adjacent water

molecules, which is confirmed by computations.⁴⁷ The low density of water in a single file and resulting high entropy were suggested⁵⁰ to be an important factor in experimentally confirmed spontaneous filling of CNTPs with water.51 However, ab initio simulations recently indicated a possibility of a significantly distorted arrangement in (6,6) CNTPs, both in the presence and absence of ions. For instance, while larger K⁺ ions were still solvated by two water molecules, smaller Na⁺ cations displayed a four-molecule solvation.⁵² Here, we find that significantly distorted arrangements in (6,6) tubes are likely even without ions.

Fig. 1a displays two arrangements of water molecules within (6,6) CNTPs, composed of a central water molecule surrounded by three other molecules on each side. Corresponding thermodynamic quantities computed by comparing CNTPs containing six and seven water molecules for each arrangement (see Methods) are shown in Fig. 1b. Fairly similar values are computed for (5,5) tubes (see the ESI†). We find that, upon energy optimization, the straight file in (6,6) tubes transforms into a zigzag arrangement shown on top of Fig. 1a. The latter has a lower energy yet still preserves the topology of the single file, as each water molecule still interacts with only two closest neighbors. However, upon energy optimization from some other initial arrangements, commensurate energies were obtained for a topologically different arrangement as shown in the bottom panel of Fig. 1a, with middle molecules bonded to three neighbors. Its energy was ~10 kJ mol⁻¹ lower than the zigzag's for six water molecules, but similarly higher for seven molecules. We trace this back to the "surface" energy of the file termini, which have the same structure for 6- and 7-member zigzags but are quite different for triple-bonded counterparts due to the seventh "under-bonded" terminal molecule. The terminal energy then cancels out in the computed water transfer energy for the zigzag but may overestimate the cost of water transfer to the triple-bonded state, which might otherwise yield a transfer energy closer to the zigzag's. For this reason, while computing ion transfer energies, we minimize this uncertainty by choosing as a reference precursor state in eqn (9) and (10) the 6-water file with (terminal) arrangement closest to one obtained around the specific ion.

Since CNTP is an open system, the water equilibrium should minimize the free energy rather than energy. We then computed for each arrangement all thermodynamic functions of water transfer, including excess transfer entropy ΔS^{ex} , excess Gibbs energy ΔG^{ex} (shown in Fig. 1b), and enthalpy $\Delta H = \Delta G^{\text{ex}} +$ $T\Delta S^{\text{ex}}$, using Gaussian's thermochemical package. Since water in CNTP is a phase co-existing with the water bulk phase, according to the Clapeyron equation, the equilibrium requires $\Delta G^{\text{ex}} = 0$. While ΔS^{ex} indicates whether a water arrangement in CNTP is more constrained than the bulk, ΔG^{ex} indicates how it compares with the equilibrium state. We focus on $\varepsilon = 2$, as the most representative of CNTPs embedded in the lipid membrane, but the numbers vary weakly with ε , since water is not charged (cf. values of ions below), see Fig. 1b.47 The negative $-T\Delta S^{\text{ex}} = -0.8 \text{ kJ mol}^{-1}$ of the zigzag arrangement indicates

Nanoscale

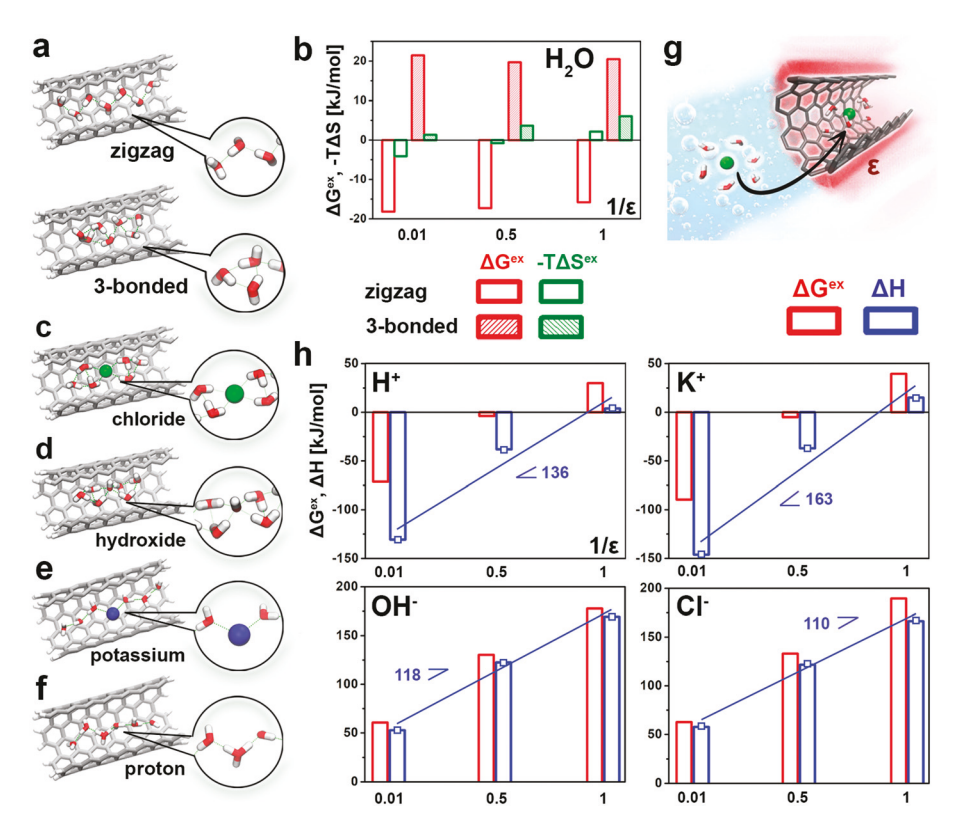


Fig. 1 Molecular arrangement and transfer quantities for water and ions in (6,6) CNTPs. (a) Zigzag (top) and triple-bonded (bottom) arrangement of water in CNTPs and (b) computed $\Delta G^{\rm ex}$ and $-T\Delta S^{\rm ex}$ for water transfer to CNTPs for each arrangement at different ε . Water arrangement around chloride (c), hydroxide (d), potassium (e) and proton (f) ions in water-filled CNTPs. (g) Schematic illustration of the single ion transfer process from bulk water to water-filled CNTPs and (h) computed transfer quantities, ΔG^{ex} and ΔH , for transfer of H⁺, K⁺, OH⁻, and Cl⁻ as single ions plotted versus 1/\varepsilon\$. The slanting line and the value of the slope highlight the effect of dielectric energy. Oxygen, carbon, and hydrogen atoms and chloride ions are depicted in red, grey, white and green, respectively.

that it is slightly less constrained (rarer) than bulk water, whereas its negative $\Delta G^{\text{ex}} = -17.3 \text{ kJ mol}^{-1}$ indicates that it is also rarer than the equilibrium one (open bars in Fig. 1b), i.e., more water is to be inserted to reach equilibrium. On the other hand, the triple-bonded arrangement has a positive $-T\Delta S^{\text{ex}} =$ 3.6 kJ mol⁻¹, *i.e.*, is denser than bulk water. Its positive $\Delta G^{\text{ex}} =$ 19.7 kJ mol⁻¹ indicates that it is also denser than the equilibrium state, i.e., some water molecules need to be expelled for reaching equilibrium (cross-hatched bars in Fig. 1b). If ΔG^{ex} is an overestimate, this arrangement is probably closer to equilibrium than the last number suggests. Nevertheless, the equilibrium arrangement in (6,6) tubes is likely to be intermediate to the zigzag and triple-bonded states, neither of which is a regular single file. Its thermodynamic properties may, in principle, be obtained by full quantum MD simulations on much larger systems but, unfortunately, fast ab initio methods suitable for MD, such as pseudopotential-based, poorly estimate bulk hydration,46 critical in the present context. On the other hand, the computational costs of MD at a higher level of theory, such as the one used here, would be formidable.

However, we may estimate the equilibrium properties by appropriately interpolating between the two arrangements. On approximating equilibrium as a superposition of the two states, each weighed by the Boltzmann factor with respective

 $\Delta G^{\rm ex}$, fractions of each state are found by requiring total $\Delta G^{\rm ex}$ = 0. The transfer enthalpy will then be effectively dictated by the state with lower ΔG^{ex} , but only a small fraction of water will be found in this arrangement (see the ESI†). While diffusing along CNTPs, water will have to assume temporarily a higher energy state. We then speculate that the triple-bonded state may represent the relevant diffusion transition state, whose enthalpy is larger by 15-20 kJ mol⁻¹ than bulk water. Indeed, Li et al. reported recently a reasonably close experimental activation energy of 20 kJ mol⁻¹ for water permeation through (6,6) CNTPs. 13

Weaker steric constraints in (6,6) tubes, compared with (5,5), also allow distortions of water arrangement around ions. Thus, the lowest energy straight-file two-molecule hydration of OH and Cl anions in (5,5) CNTPs⁴⁷ transforms upon optimization to a different, four-molecule hydration with lower energy within (6,6) CNTP, as shown in Fig. 1c and d. This might partly be due to the repulsive interaction of anions with CNT walls, thereby anions tend to assume a position near the CNT main axis, which makes them sterically more accessible for hydration (see Fig. S4d in the ESI†). In contrast, cations show a far more attractive interaction with CNT walls and thus tend to assume an eccentric position (Fig. S4c†), sterically less accessible for hydration. Then, in agreement with other

reports, 52 two-molecule hydration was found here for K and H (essentially, H₃O⁺) cations (Fig. 1e and f). Since the energy of internal hydration is a considerable part of the total ion transfer energy, e.g., about 50% for K⁺ and 25% for Cl⁻ in (5,5) tubes, ⁴⁷ this difference may affect the energy of ion transfer from water to CNTPs. Nevertheless, unlike the case of CNT(5,5), 47 electrondensity maps in Fig. S4† show a negligible overlap between the π -electrons of CNT(6,6) and electron clouds of water or ions. This suggests that the interaction between the π -electron system of CNTPs and ions is mainly electrostatic, favorable for the cations and unfavorable for anions.

How much does it cost to transfer ions?

Fig. 1e and f illustrate the ion transfer process and display the key transfer quantities, excess Gibbs energy $\Delta G^{\rm ex}$ and enthalpy ΔH , for moving ions into water-filled (6,6) CNTPs (complete data and a comparison with (5,5) tubes are presented in the ESI, Fig. S3†). These quantities are plotted versus $1/\varepsilon$ and the slope highlights the contribution from the dielectric energy, the polarization of the medium surrounding CNTPs, 47 which adds a significant cost to ion transfer. It reaches a maximum in vacuum ($\varepsilon = 1$) and vanishes when ε reaches infinity, i.e., at $1/\varepsilon = 0$. Neither of these extremes reflect typical experimental conditions, yet ε = 2 (1/ ε = 0.5) may reasonably represent lipid membranes⁵³ embedding CNTPs in most experiments. The slopes for the anions are somewhat smaller than those for cations. This may be a result of more favorable electrostatic interaction of cations with the CNTP electron cloud and charge redistribution, decreasing the dielectric energy.47 Yet, the slopes of all ions are reasonably close and similar to results for (5,5) CNTPs (ESI, Fig. S3†). This contribution is then about rigid shifts of $\Delta G^{\rm ex}$ and $\Delta H^{\rm ex}$ of all ions relative to ion-specific base values.

Compared to its effect on water transfer, ΔS^{ex} seems to play a smaller role in ion transfer, therefore $\Delta G^{\rm ex}$ is mainly controlled by enthalpy. Due to more favorable interaction with CNTPs, cations have significantly lower transfer energy than anions. For instance, for $\varepsilon = 2$, K⁺ transfer to CNTPs is nearly athermal and, for (6,6) tubes, it is even more favorable than the transfer of water, while the transfer of anions is highly unfavorable. Enhanced interaction of potassium was already noted by Aydin et al. for slightly wider tubes and is reminiscent of the long-known complexation of cations with benzene, "cation- π interaction".⁵⁴ Partly but less significantly, the differences between the ions are also related to different arrangements of water molecules and water-water interaction around the ion, different for cations and anions. We also note that a proton transfers about as favorably as K⁺. Practically, that means that, in experiments that involve KCl solutions, K⁺ will outcompete the more dilute protons and must be the dominant cation species within CNTPs.

However, uptake of K⁺ is subject to limitations imposed by the requirements of overall electroneutrality. The latter will always apply whenever potential variations in CNTPs are

sufficiently smeared by either the screening length being shorter than CNTP length⁵⁵ or ion charge delocalization via bonding to CNTPs. 47 Electroneutrality dictates that the uptake of a K⁺ cation needs to be counter-balanced by the uptake of an anion, either Cl or OH, both having a highly unfavorable $\Delta G^{\rm ex}$. As the simplest mean-field approximation, we may assume a uniform mean potential φ within the CNTP relative to bulk thus ion uptake is given by

$$\sum_{i \text{(cations)}} C_i \exp\left(-\frac{\Delta G_i^{\text{ex}} + F\phi}{RT}\right) = \sum_{j \text{(anions)}} C_j \exp\left(-\frac{\Delta G_j^{\text{ex}} - F\phi}{RT}\right),\tag{1}$$

where C's are respective cation and anion concentrations in solution. The exponents are essentially ion partitioning coefficients, calculated by solving this equation for φ , given ΔG^{ex} for all ions. ΔG^{ex} should be understood as the appropriate statistical means, reflecting ion-ion interactions as well. Yet, in the simplest picture, when ions are assumed to collectively preserve electroneutrality but, otherwise, do not significantly interact with each other, we approximate ΔG^{ex} by the values computed for individual free ions. We consider available experimental data on ion transport in CNTPs along with the present ab initio results to judiciously select the ions that need to be considered in eqn (1). Most measurements yield ion permeabilities rather than partitioning, therefore the differences in ion mobilities need to be considered as well. However, as water in the 0.8 nm CNTP is still not too much more constrained compared with bulk water and neither are ions, their mobility should not drastically differ from the bulk values. Indeed, the inspection of reported estimates of water diffusion within (6,6) tubes obtained by experiments and simulations show that virtually all of them vary within a fairly narrow range between 0.89 and 4.4×10^{-9} m² s⁻¹. This range contains even a more narrow range from 1 to 2.5×10^{-9} m² s⁻¹ covering all reported diffusivity values for water and potassium and lithium cations in 1 and 1.5 nm tubes, as well as bulk mobilities of these species and chloride (see the ESI†). Proton and hydroxide ions are well-known exceptions, as they employ the much faster Grotthuss mechanism. MD simulations by Lee et al., modified to allow water dissociation, placed diffusivities of both ions in (6,6) tubes in the similar range of 19 to 32 \times 10⁻⁸ m² s⁻¹, with smaller values corresponding to shorter tubes. 56 Dellago et al. obtained a fairly close value 17×10^{-8} m² s⁻¹ for protons using *ab initio* computations.⁵⁷ Notably, the uncertainties for water and regular ions stay within a factor of 5 from each other and, for proton and hydroxide, within a factor of 2. On the energy transfer scale, this is equivalent to 4 and 2 kJ mol⁻¹, respectively, i.e., within the error of ab initio computations. Given such insignificant uncertainties of mobilities, we deem it most expedient to simply adopt for subsequent calculations the bulk values 2×10^{-9} m² s⁻¹ for potassium and chloride mobilities and, for hydroxide, Lee et al.'s estimate for shortest (6,6) tubes, 24×10^{-8} m² s⁻¹.

When KCl transfers as free ions subject to electroneutrality and the effect of pH is negligible, i.e., H⁺ and OH⁻ do not Nanoscale

affect salt uptake, K⁺ and Cl⁻ hence salt concentrations within CNTPs, denoted with a bar, will all be about identical and linearly depend on the salt concentration in solution C_s , as follows

$$\tilde{C}_{\rm s} = \tilde{C}_{\rm K} = \tilde{C}_{\rm Cl} = C_{\rm s} \, \exp\left(-\frac{\Delta G_{\rm K}^{\rm ex} + \Delta G_{\rm Cl}^{\rm ex}}{2RT}\right).$$
 (2)

The average $\Delta G_{\rm s}^{\rm ex} = \frac{1}{2} \left(\Delta G_{\rm K}^{\rm ex} + \Delta G_{\rm Cl}^{\rm ex} \right)$ essentially plays here the role of excess Gibbs energy for pH-independent salt transfer. However, the non-linear scaling of conductivity observed at pH 7.5 in Fig. 2a indicates that such a pH-independent scenario operates only at low pH. Apparently, pH comes into play under neutral conditions as preferential uptake of OH⁻ ions, as reported for wider tubes and observed in ab initio simulations of graphene surfaces in water.^{27,58} When OH⁻ is strongly favored over Cl⁻, eqn (1) has to be replaced with

$$\bar{C}_{\rm K} \approx \bar{C}_{\rm OH} \approx \left(C_{\rm s}C_{\rm OH}\right)^{1/2} \exp\left(-\frac{\Delta G_{\rm K}^{\rm ex} + \Delta G_{\rm OH}^{\rm ex}}{2RT}\right),$$
(3)

where $C_{\rm OH} = 10^{\rm pH-14}$ is in M units. The unusual 1/2 scaling of conductivity with C_s predicted by eqn (3) and observed by Tunuguntla et al. at pH 7.5 is a signature of such a pH-dependent ion partitioning.³⁵ In this scenario, potassium mainly transfers in combination with hydroxide, i.e., KOH, with a transfer energy $\Delta G_{\rm h}^{\rm ex} = \frac{1}{2} \left(\Delta G_{\rm K}^{\rm ex} + \Delta G_{\rm OH}^{\rm ex} \right)$ replacing $\Delta G_{\rm s}^{\rm ex}$. On the other hand, Cl⁻ will transfer as a trace species and its concentration in CNTPs will be given by

$$\begin{split} \bar{C}_{\text{Cl}} \approx & {C_{\text{S}}}^{3/2} {C_{\text{OH}}}^{-1/2} \ \exp \left(-\frac{2\Delta G_{\text{Cl}}^{\text{ex}} + \Delta G_{\text{K}}^{\text{ex}} - \Delta G_{\text{OH}}^{\text{ex}}}{2RT} \right) \\ = & {C_{\text{S}}}^{3/2} {C_{\text{OH}}}^{-1/2} \ \exp \left(-\frac{2\Delta G_{\text{S}}^{\text{ex}} - \Delta G_{\text{h}}^{\text{ex}}}{2RT} \right), \end{split} \tag{4}$$

Since, as the minority species, Cl- controls KCl permeability in this regime, the salt and Cl⁻ permeation rates should scale with salt concentration as $C_s^{3/2}$ and the quantity $\Delta \tilde{G}_{\rm s}^{\rm ex} = \Delta G_{\rm s}^{\rm ex} - \frac{1}{2} \Delta G_{\rm h}^{\rm ex}$ should replace $\Delta G_{\rm s}^{\rm ex}$ for chloride transfer in this scenario. Along with the 1/2 scaling of conductivity, these features are another signature of the pH-controlled ion transfer. Obviously, when OH concentration decreases, e.g., by 4.5 orders of magnitude at pH 3, this regime should transition to "regular" linear KCl transfer.

Li et al.46 measured chloride permeation rates using the stop-flow experiment in vesicles and derive chloride permeability in CNTPs P_{Cl} by fitting the anion permeation rate to a linear dependence on $C_{\rm s}$. However, the observed trend was clearly non-linear and a much better fit is obtained for $C_8^{3/2}$ scaling, in agreement with eqn (4), as shown in Fig. 2b (see also the ESI, Fig. S5†). We also find that the computed $\Delta \tilde{G}_{s}^{\text{ex}} =$ 62.6 kJ mol⁻¹ (for $\varepsilon = 2$) fully agrees with the value of 63 kJ mol⁻¹ obtained by viewing it as a parameter and fitting eqn (4) with mobilities estimated as explained above to measured permeation rates shown in Fig. 2b. We also note that P_{Cl} of chloride derived from the above stop-flow anion permeation experiments in vesicles for similar solution compositions at pH 7.5 is of the order 10^{-18} – 10^{-17} cm³ s⁻¹, equivalent to conductance $\frac{F^2}{RT}C_{\rm Cl}P_{\rm Cl}$ of a few fS per channel. On the other hand, electrical measurement by Tunuguntla et al. in Fig. 2a shows a much larger electrical conductance of the order 2-30 pS per channel at this pH. These authors also estimated ion transport numbers using reverse potential measurements.²⁵ The potassium transport number $t_{\rm K}$ was found to be under 0.1 at pH 7.5, reasonable when the rest of the current is carried by highly mobile hydroxide. The small chloride permeability measured in stop-flow experiments at pH 7.5 is then another manifestation of chloride being a minority anionic species within CNTPs at this pH. Yet, $t_{\rm K}$ increased to about 0.65-0.85 at pH 3, as expected when chloride takes over as the dominant anion.

Here, we note that the above results also rule out the alternative mechanism, often discussed in the context of ion selectivity in CNTPs, whereby weakly acidic groups at the rim are presumed to repel anions and thus control ion transfer. As

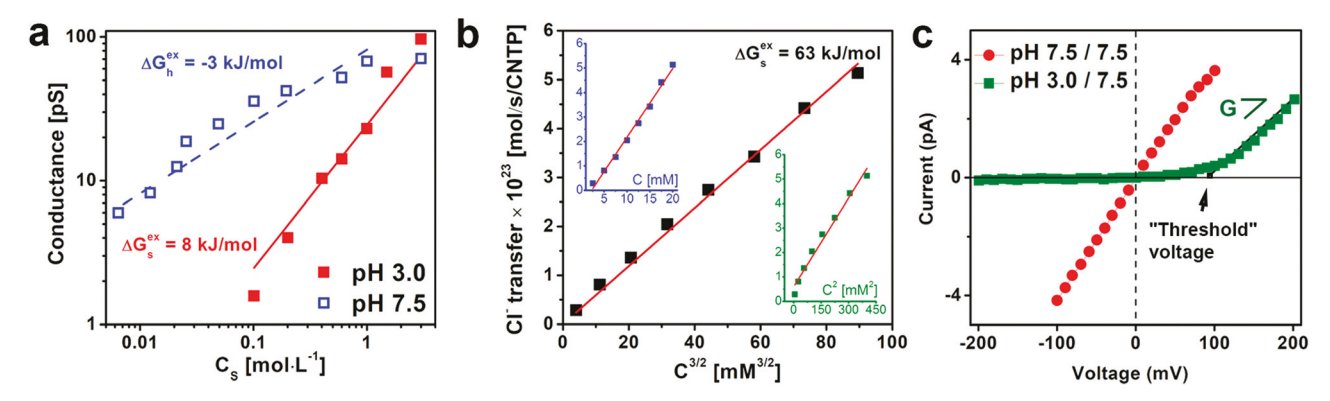


Fig. 2 Key experimental results on ion transport in 0.8 nm CNTPs. (a) CNTP conductivity in KCl solutions at pH 3 and 7.5 reported by Thunuguntla $et~al.^{25}$ Solid and dashed lines were computed using, respectively, eqn (2) and (3) with mobilities estimated based on Dellago $et~al.^{57}$ and ΔG_s^{ex} and ΔG_h^{ex} viewed as an adjustable parameter with the best-fit value indicated. (b) Rate of chloride permeation per CNTP measured in vesicles at pH 7.5 vs. $C_s^{3/2}$, as reported by Li et al. 13 Solid line is a linear fit to eqn (4) with mobilities estimated based on Dellago et al. 57 and $\Delta \tilde{G}_s^{sx}$ viewed as fitting parameters with the best-fit value indicated. The insets highlight non-linear dependence obtained by plotting the same data vs. C_s and C_s^2 . (c) Current– voltage dependence of CNTPs connecting two 0.1 M KCl solutions of pH 3 and 7.5 (green squares) and of the same pH 7.5 (red circles), reported by Tunuquntla et al.²⁵ All data were digitized from original reports.

the acidic charges are active at pH 7.5 and neutralized at pH 3, the anion permeation should be more suppressed at higher pH and their transport number should drop and that of cations increase. This clearly disagrees with observations, as Li et al. report that permeation rates of chloride and other halides do not change significantly between the two pH values.46 Along with conductivity measurements of Tunuguntla et al. showing a much larger cation transport number at lower pH,²⁵ this makes it unlikely that acidic groups at the rim contribute significantly to ion transfer resistance.

In another report, Tunuguntla et al. employed permeation in vesicles loaded with a pH sensitive dye at pH 7.5 to measure proton transfer rates in CNTPs under a pH gradient.²⁶ The observed rates were interpreted as a fast proton transfer, presumably involving the Grotthuss mechanism. We note, however, that proton flux $J_{\rm H}$ is indistinguishable from the oppositely directed transfer of hydroxide J_{OH} or simultaneous transfer of both ions in the form of alkalinity flux J_{OH} - J_{H} . The present analysis strongly suggests that the actual permeating species was OH-. The higher affinity of narrow CNTPs to hydroxide also readily explains their larger conductivity, compared with wider 1.5 nm CNTPs. The measured rate of alkalinity transfer is equivalent to a conductance of the order 1 fS, again, corresponding to anion transfer data, yet four orders of magnitude smaller than the results of conductivity measurements. This discrepancy manifests coupling of alkalinity transfer, i.e., OH⁻ permeation to a much slower transfer of K⁺. In the absence of electric current, its rate is limited by K⁺ diffusivity and may no more benefit from the fast Grotthuss mechanism. The reported blocking effect of Ca2+ is also consistent with this picture, as it should bind to CNTP more strongly and have a lower mobility than K⁺ due to double charge and thus further slow down hydroxide permeation.

Finally, activation energies E_a of permeation offer yet another way of comparing the present model with experiments. They should be dominated by the enthalpies of ion transfer, i.e., ΔH , displayed in Fig. 1h as well. For instance, Li et al.13 reported activation energies for the permeation of halide anions, however, the present model indicates they may not be compared directly with ΔH for respective anions due to coupling to other ions. Thus, depending on whether eqn (2) or (4) describes chloride transfer, the apparent activation energy for Cl⁻ permeation should be - using notation analogous to $\Delta G^{\rm ex}$ – either $\Delta H_{\rm s}$ or $\Delta \tilde{H}_{\rm s}$, respectively. Li et al. reported $E_{\rm a}$ = 52 kJ mol⁻¹ for chloride permeation in vesicles, which they compared with computed chloride transfer energy 63 kJ mol⁻¹. It is unclear why the latter value, computed for CNTPs in vacuum ($\varepsilon = 1$), is so different from the present $\Delta H_{\rm Cl} \approx 166$ kJ mol^{-1} for $\varepsilon = 1$ and is much closer to the present result for $\varepsilon =$ 100. We presume this might be affected by the fact that, in computations by Li et al., CNTPs were connected to highly polarizable graphene sheets, which could strongly reduce the dielectric contribution by essentially "grounding" the CNTPs. Nevertheless, the activation energy of chloride transfer may not be identified with $\Delta H_{\rm Cl}$ in either case and the agreement could be fortuitous.

The present analysis suggests that the observed $E_a = 52 \text{ kJ}$ mol⁻¹ of chloride permeation should be compared with either $\Delta H_s \approx \frac{1}{2}(-37.1+121.7) = 42.3 \text{ kJ mol}^{-1} \quad \text{for the } \quad \text{pH-indepen-}$ dent scenario, eqn (2), or with $\Delta \tilde{H}_s = \Delta H_{Cl} + \frac{1}{2}(\Delta H_{K} - \Delta H_{OH}) \approx$ $121.7 + 0.5 \times (-37.1 - 122.4) = 42.0 \text{ kJ mol}^{-1}$ for the pH-controlled one, eqn (4). These values are close, due to similar transfer energies for chloride and hydroxide and may not differentiate between the two theoretical expressions, however, the scaling of the conductivity and permeation rate with C_s shown in Fig. 3 strongly favors $\Delta \tilde{H}_{\rm s}$ as the appropriate one. The difference between the observed E_a and appropriate ΔH may come from not accounting for the activation energy of diffusion, which may be fairly close to that of water discussed above, 15-20 kJ mol-1, and add to E_a accordingly. On the other hand, sensitivity to ε (see Fig. 2) presents another substantial uncertainty. For instance, replacing $\varepsilon = 2$ with $\varepsilon = 2.4$, better representing lipids, ⁵³ reduces ΔH by about 20 kJ mol⁻¹.

In a similar manner, eqn (4) predicts that the activation energy for alkalinity permeation should be $\Delta H_h = \frac{1}{2}(\Delta H_K +$ $\Delta H_{\rm OH}) \approx 0.5 \times (-37.1 + 122.4) = 42.6 \, {\rm kJ \ mol^{-1}} \ {\rm for} \ \varepsilon = 2$. This is fairly close to the experimental value of 55 kJ mol⁻¹ reported by Tunuguntla et al.25 The difference could again come from unaccounted for activation energy of diffusion and the sensitivity of transfer energies to ε . Another factor is deviations from the simple mean-field picture, i.e., ion-ion interactions that should reduce the transfer energies, as analyzed next.

The puzzle of hydroxide: why it is favored and how it conducts

The above comparison with experiments demonstrates that computed values of ΔG^{ex} for free ions combined with simple mean-field relations may rationalize most experimental observations and trends. However, two points raise questions. First, despite the fact that the C_s scaling of experimental data in Fig. 2 strongly suggests that CNTP has a strong preference for hydroxide, transfer energies of single chloride and hydroxide anions shown in Fig. 1h do not display as much difference. In addition, viewing $\Delta G_s^{\rm ex}$ and $\Delta G_h^{\rm ex}$ as adjustable parameters and fitting them to the conductivity data at pH 3 and 7.5 using eqn (2) and (4), respectively, yields $\Delta G_{\rm s}^{\rm ex} \approx 8 \text{ kJ mol}^{-1}$ and $\Delta G_{\rm h}^{\rm ex} \approx$ -3 kJ mol⁻¹ that are significantly different from the present ab initio estimates (see Fig. 2a and the ESI† for details). We may only speculate below as to why these fits deviate so much from theoretical values that, otherwise, reasonably agree with the stop-flow permeation data. However, the much different fitted ΔG_s^{ex} and ΔG_h^{ex} once again manifest a high affinity of CNTP to hydroxide and it is necessary to consider more involved scenarios that would favor this ion.

Second, concurrent permeation of free cations and anions, like in stop-flow experiments in vesicles, may proceed with minimal mutual interference, however, in electrical measureNanoscale Paper

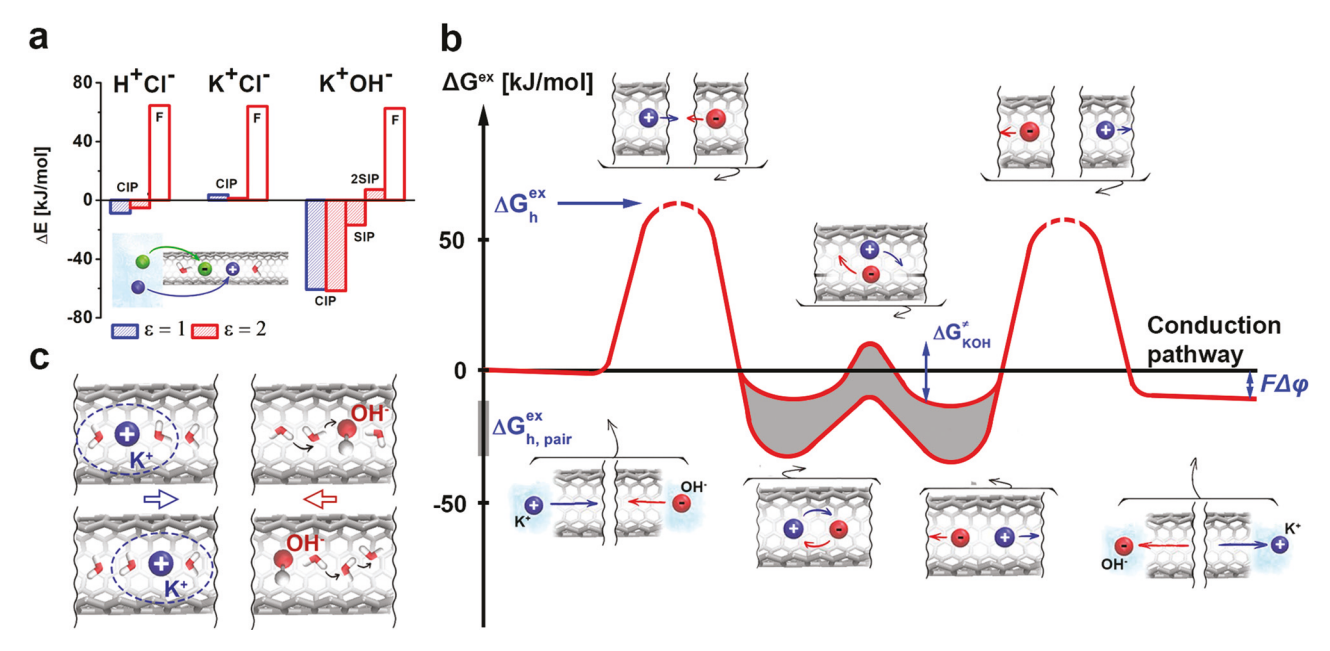


Fig. 3 Ion pair formation and conduction mechanism in (6,6) CNTPs. (a) ΔG^{ex} of ion-pair formation in CNTPs for different ion pairs for $\varepsilon = 1$ and $\varepsilon = 2$; F denotes free ions, CIP contact pairs, SIP – pair separated by one water molecule, 2SIP – pair separated by two water molecules. (b) Schematic energy profile encountered by the potassium and hydroxide ions along the conduction pathway, including free-ion uptake, downfield migration, transient pair formation, flip, and dissociation. (c) Possible mechanism of electro-osmosis: water flow coupled to potassium migrations and decoupled from hydroxide migrating by the Grotthuss mechanism.

ments, ions migrate in opposite directions and, at some point, meet and need to pass each other. It is not obvious whether squeezing ions passing each other in a narrow channel does not present a prohibitive kinetic barrier. Admittedly, this barrier would be eliminated in a scenario recently analyzed by Levy et al. who argued that electroneutrality could break down in a narrow and short channel thereby ions could pass the entire channel one at a time.⁵⁵ This mechanism was justified on the ground that screening length in a CNTP becomes exponentially large due to one-dimensionality of the "solution" in a narrow channel. However, in such a scenario, K⁺ transfer as a lone charge carrier would be decoupled from OH and, instead, coupled to Cl-. Indeed, we do not anticipate any ionspecific effect in solution outside CNTPs therefore far more dilute hydroxide would be unable to outcompete chloride and would have a negligible effect on potassium transfer. Conversely, hydroxide transfer as a lone species within CNTPs must be strongly suppressed by its prohibitive transfer energies (Fig. 1h), which disagrees with its high transfer number. It seems that experimental data and present ab initio results rule out the electroneutrality breakdown mechanism.

A more plausible alternative is that the system may substantially deviate from the simple mean-field picture due to ionion interactions. Specifically, when ions approach each other, the electrostatic part of the highly unfavorable interaction of anions with CNTPs may be attenuated or, when ions associate, eliminated and thus ion-specific effects may come into play. As a proxy of such situation, we consider ion pairing, thereby ions within CNTPs may be present as coexisting pairs and free ions. Essentially, this model is a one-dimensional analogue of

the Bjerrum model of electrolyte solutions, in which ions pairs coexist with a free-ion solution treated in the mean-field manner. ⁵⁹ Although the need for squeezing cation and anion past each other to allow conduction may not be avoided, OH uptake as a paired ion could become more favorable and reduce the corresponding barrier as well. Analyzing this scenario requires transfer energies for pairs formed within CNTPs, which we compute here *ab initio*.

Fig. 3a shows transfer energies of the possible contact ion pairs (CIP) in (6,6) CNTPs in a vacuum and ε = 2, along with the transfer energy of the same combination as free non-interacting ions (F), i.e., the average of the two single-ion transfer energies, shown as empty bars. To reduce computational costs, we simply consider the electronic transfer energy ΔE , given ΔE and $\Delta G^{\rm ex}$ show identical trends and reasonably small differences for free ions (see the ESI†). It is immediately notable that the KOH pair has an exceptionally low transfer energy compared to the other pairs, which may now rationalize the strong preference of narrow CNTPs for OH over Cl . Similar to water, which is formally the H^+/OH^- pair, the transfer energies of all ion pairs ΔE_{pair} are weakly affected by ε . Compared to the transfer energy of the pair as free ions, i.e., $\frac{1}{2}(\Delta E_+ + \Delta E_-)$, there is a gain of several tens of kJ mol⁻¹ for all salts. However, ΔE or ΔG^{ex} for pairs and free ions may not be directly compared, since pairing also involves a significant entropy loss. Considering dilute solutions and neglecting the solution non-ideality and different sizes of ions and pairs, the concentration of KOH pairs in CNTPs is given by

$$\bar{C}_{\text{KOH}} = \frac{C_{\text{K}}C_{\text{OH}}}{C_{\text{w}}} \exp\left(-\frac{\Delta G_{\text{KOH}}^{\text{ex}}}{RT}\right),\tag{5}$$

where $C_{\rm w}$ = 55.6 M in the denominator comes from the fact that the ideal solution entropy needs to be computed using concentrations expressed in molar fractions. We compare eqn (2) and (5) and, specifically, consider the exponential factor that multiplies in eqn (2) the product $(C_K C_{OH})^{1/2}$ that gauges the activity of the KOH "salt" in solution. This shows that the free-ion transfer energy $\Delta G_{\rm h}^{\rm ex} \approx 62.6 \text{ kJ mol}^{-1}$ (for $\varepsilon = 2$) in eqn (2) is to be compared with $\Delta G_{\text{h,pair}}^{\text{ex}} = \Delta G_{\text{KOH}}^{\text{ex}} + RT \ln[C_{\text{w}}/(C_{\text{K}}C_{\text{OH}})^{1/2}]$ for KOH uptake as ion pairs. The second term in the last expression accounts for the loss of translational entropy upon pairing and, for C_s in the range from 10^{-3} to 1 M and $3 \le pH \le 7$, it amounts to about 30 to 50 kJ mol⁻¹. To complete this analysis, we obtained using Gaussian's thermochemical package $\Delta G_{\text{KOH}}^{\text{ex}} = -61.6 \text{ kJ mol}^{-1}$ for $\varepsilon = 2$, which turns out to be only slightly above ΔE_{KOH} (see Fig. 3). Ultimately, the terms sum up to $\Delta G_{\rm h,pair}^{\rm ex} \approx -31$ to -11 kJ mol⁻¹ for the above composition range. It is obviously far below the free-ion counterpart and indicates that a majority of K⁺ and OH ions partition to CNTPs as KOH pairs.

Similar analysis for the other pairs shows that, even if their formation is not as favorable as KOH, they are likely to contribute at least as much as the corresponding combination of free ions (CIP vs. F bars in Fig. 3a). While pairs represent only the simplest form of ion-ion interactions deviating from mean-field treatment, the present analysis highlights the crucial role of such interactions in controlling ion partitioning and transport in CNTPs and, in particular, high affinity towards OH-. We note, however, that the presence of pairs in CNTPs does not necessarily directly translate into transport, since pair mobility may be small. Indeed, we note that, in the case of chloride permeation, if this ion was mainly transferred as KCl pairs, its permeation rate would be proportional to C_s squared. The inset in Fig. 2b (see also Fig. S5 in the ESI†) indicates that this scaling disagrees with the experiment, ruling out the question of any significant contribution of ion pairs to ion permeation by diffusion.

CNTP conductance: what is the rate-controlling step

Even if abundant within CNTPs, pairs may not contribute to conductance not only due to low mobility, but also because they are neutral and cannot carry electrical current. A cation and an anion migrating in an electric field in the opposite directions may then temporarily form a pair, however, it will have to flip and split up thereafter to let the ions keep migrating. In the spirit of the Eyring-Polanyi transition-state theory, we may consider the flip and its Gibbs energy $\Delta G_{\text{KOH}}^{\text{I}}$ relative to the "ground state" of the pair aligned parallel to the main CNTP axis. Presumably, the height of the kinetic barrier corresponds to the pair aligned perpendicular to the CNTP main axis. We estimated this height to be $\Delta G_{\text{KOH}}^{\text{T}} \approx 23 \text{ kJ}$ mol^{-1} above the "ground state" $\Delta G_{\text{h,pair}}^{\text{ex}}$, which places the barrier height at -8 to 12 kJ mol⁻¹ relative to the solution. It is well below the free-ion energy $\Delta G_{\rm h}^{\rm ex} \approx 62.6 \; {\rm kJ \; mol^{-1}} \; (\varepsilon = 2)$. We then conclude that CNTP conductance should indeed be con-

trolled by the partitioning and transport of free ions, in agreement with most experimental data. Fig. 3b schematically depicts the suggested pathway and energy profile encountered jointly by the potassium and hydroxide ions upon conduction. It starts from their uptake as free ions from solution at opposite ends of CNTPs, followed by free-ion migration, pair formation, flip, dissociation back to free ions, and, ultimately, exit to the solution at the opposite end. The entire profile is slightly inclined due to the electric potential difference applied along the nanotube $\Delta \varphi$ and the shown sequence may repeat, if the CNTP contains more than one pair. The larger number of KOH pairs relative to other possible pairs, due to exceptionally low $\Delta G_{\text{KOH}}^{\text{ex}}$, is apparently the reason behind the hydroxide dominating ion conductance under neutral conditions.

One may ask what happens to water molecules within CNTPs when K⁺ and OH⁻ (or Cl⁻) migrate in an electric field and induce an electro-osmotic flow of water, as demonstrated for wider 1.5 nm CNTPs. 40 The partitioning-controlled scaling of conductivity with C_s suggests electro-osmosis in single-digit CNTPs is apparently not as strong as in wider tubes. Yet, if both ions experience strong friction with water, ions will hinder each other's migration. Indeed, when the ion with the larger friction dictates the ultimate direction of electroosmosis, the other will be forced to squeeze past all water molecules, in a manner similar to the ion pair flip. However, the Grotthuss mechanism may help circumvent this obstacle, permitting a nearly friction-less OH transfer as a fast shuttling of electrons and hydrogen between OH and a neighboring water molecule followed by minor local atom rearrangement. This may readily occur against water flow and will not interfere with the electro-osmosis induced by K+ migration, minimizing this ion's friction with water as well. This mechanism, whereby OH ions may rapidly migrate downfield regardless of electroosmosis induced by potassium, is schematically illustrated in Fig. 3c and may explain insignificant electro-osmosis in (6,6) tubes and the large transport number of OH⁻ at pH 7.5. Note that, within this picture, the ion pair flip is still required, otherwise K⁺ will separate between the OH⁻ ion and next water molecule and prevent the shuttling of electrons and hydrogen.

At this point, we note that, in reality, there is obviously no sharp distinction between free ions and pairs assumed in our highly simplified picture. The long-range nature of the electrostatic attraction between cation and anion must smear the heights and valleys of the profile in Fig. 3b. Perhaps more importantly, the ion-ion interaction should both eliminate a part of the dielectric energy and allow anions to interact more favorably with CNTP walls. This should reduce the free-ion transfer energy well below the simple combination of singleion transfer energies. To illustrate this point, we also computed and display in Fig. 3a the transfer energies of the KOH pairs separated by one (SIP) and two (2SIP) water molecules. The transfer energy clearly increases with ion-ion separation, but it may still remain noticeable below the free-ion value over distances of a few nanometers, reducing the average transfer energy. This might partly explain why very low $\Delta G_{\rm s}^{\rm ex}$ and $\Delta G_{\rm h}^{\rm ex}$ fitted to conductance data shown in Fig. 2a are closer to ΔG^{ex}

Nanoscale Paper

for corresponding pairs with pairing entropy correction than to their free-ion counterparts. On the other hand, the rates and activation energies of chloride and alkalinity permeation measured in stop-flow experiments agree better with the simple free-ion estimates. Not unlikely, part of the answer may have to deal with the fact that the conductivity is controlled by the faster ion of the pair, *i.e.*, OH^- in the case of KOH, while the permeability measured in stop-flow experiments is determined by the slower one, *i.e.*, K^+ . We also speculate that effects absent or ignored in the present analysis, *e.g.*, alternative conduction paths, or different settings and the CNTP environment in electrical and stop-flow measurements, changing the effective value of ε , may affect the results. We presume these questions will be clarified, as more data on ion transport in CNTPs become available.

Current rectification explained

Finally, we will show that the strong dependence of conductance on OH^- readily explains current rectification between solutions of different pH values and, specifically, blockage of current in the direction from low to high pH. The mean-field relation, eqn (3), may be incorporated into Nernst–Planck-type relations, which yields the following relation between the current (I) and applied voltage ($\Delta \varphi$) and solution composition differences (see the ESI† for derivation)

$$I = G\left(-\Delta\varphi + t_{\text{OH}} \frac{RT}{F} \Delta \ln C_{\text{OH}} - t_{\text{K}} \frac{RT}{F} \Delta \ln C_{\text{K}}\right), \qquad (6)$$

where Δ designates differences between the two solutions and $t_{\rm OH}$ and $t_{\rm K}$ are respective ion transport numbers within CNTPs. G is the effective CNTP conductivity, having the following dependence on the solution concentrations

$$G \propto \frac{\Delta (C_{\rm K} C_{\rm OH})^{1/2}}{\Delta \ln (C_{\rm K} C_{\rm OH})^{1/2}} = \left\langle (C_{\rm K} C_{\rm OH})^{1/2} \right\rangle_{l.m.},$$
 (7)

where the omitted proportionality constant accounts for the partitioning (related to the transfer energies), ion mobilities and CNTP geometry. Eqn (7) shows that G is proportional to the logarithmic mean of the products $(C_K C_{OH})^{1/2}$ of the two solutions, thereby it is mainly determined by the solution with the larger $(C_K C_{OH})^{1/2}$. For instance, in experiments by Tunuguntla et al.,25 displayed in Fig. 2c, current rectification was observed between solutions with pH 7.5 and 3 containing 0.1 M KCl on both sides (green squares). The driving force, i.e., expression in brackets in eqn (6), depends on both pH values and becomes zero when the applied potential equals the threshold voltage, as indicated in Fig. 2c. Above this potential, the conductance G, i.e., the I-V slope, determined by pH 7.5, is indeed similar to the case when both solutions have the same pH 7.5 (red circles in Fig. 2C). However, the conductance sharply drops and the current is blocked below this potential due to local pH changes induced by polarization.

Eqn (6) and (7) predict no rectification, yet it may come from concentration polarization, *i.e.*, ion depletion or enrich-

ment in solution next to the CNTP mouth, when a DC current enters or exits CNTP. The above rectification experiments were performed in the presence of large concentrations of salt. The transport of salt ions, in particular, potassium is then not a limiting factor and the key limitation comes from the depletion of OH⁻ ions in solution next to a CNTP mouth. The large salt concentration also facilitates the analysis, since it eliminates the potential gradients in the solution. Thus the depletion or enrichment of OH is controlled primarily by its diffusion away from or towards CNTPs and the magnitude and direction of the flow of OH ions, i.e., the fraction of the current carried by OH⁻, It_{OH}. Different situations encountered in conduction and rectification experiments are schematically illustrated in Fig. 4. To obtain the limiting value of It_{OH} and total current, the semi-spherical boundary layer of solution centered at the CNTP mouth is considered. The OH concentration at the mouth will depend on It_{OH} and the bulk concentration as follows14

$$C_{\text{OH,mouth}} = C_{\text{OH,bulk}} \pm \frac{It_{\text{OH}}}{2\pi F D_{\text{OH}} r_{c}},$$
 (8)

where D_{OH} is the OH⁻ diffusivity in solution, r_c is the channel radius, and the sign is positive or negative when OH ions move away from or towards the CNTP. According to eqn (7) conductivity will be controlled by the higher pH faced by CNTPs, marked with the star Fig. 4. Thus the higher pH will always increase and the current will flow unobstructed, when CNTPs face two identical solutions (Fig. 4a). Similarly, no blockage will be observed when the current - by definition, opposite to OH⁻ flow - is towards the low-pH solution, since it increases $C_{OH, mouth}$ at the high-pH end and hence G, as shown in Fig. 4b. However, as depicted in Fig. 4c, when the current reverses, $C_{OH, mouth}$ at the high-pH end drops, sharply reducing G and blocking the current. Since chloride does not allow as much conductivity as hydroxide (cf. Fig. 2a), we ignore the takeover by chloride at low pH and take the maximal (limiting) current I_{lim} as approximately corresponding to C_{OH} , $_{\text{mouth}} = 0$. Using $D_{\text{OH}} = 6.8 \times 10^{-9} \text{ m}^2 \text{ s}^{-1}$, $r_{\text{c}} = 0.4 \text{ nm}$, $t_{\text{OH}} = 0.9$, and $C_{\rm OH,\ bulk}$ = $10^{-6.5}$ M (pH 7.5), we estimate $I_{\rm lim}$ = $(2\pi FD_{\rm OH}r_{\rm c}C_{\rm OH,\ bulk})/t_{\rm OH}\sim 1$ fA, which is far smaller than pA currents measured in the forward direction, thereby the backward current will be effectively blocked, i.e., rectification will be observed. More accurate relations, accounting for the pH changes at both ends and yielding the entire I-V curve may be easily developed, by combining eqn (6) and (7) with mass transfer in solutions, 14 but they do not change the above conclusion. Note, the full model must also address the fact that It_{OH} flows in solution as an alkalinity flow, carried by both OH and H. The effective diffusivity of OH, yielding the total alkalinity flux, then becomes pH-dependent, D_{OH} + D_{H} 10^{14-2pH}. Obviously, the actual species carrying the most alkalinity flow in pH 3 solution (and, in general, at any pH \leq 7) is H⁺ rather than OH⁻, as indicated in Fig. 4b and c.

At this point, we note that the very small limiting current (*i.e.*, large access resistance) of OH⁻, responsible for current rectification, is due to its very low concentration in solution at

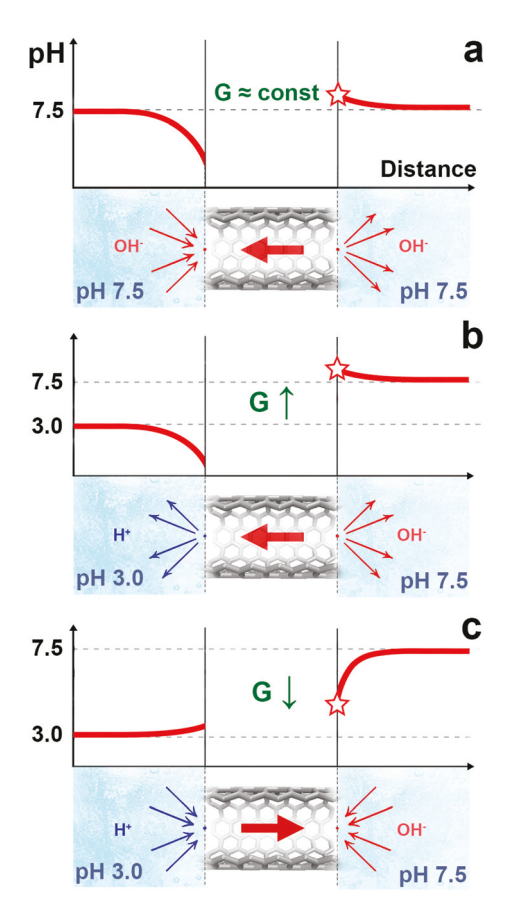


Fig. 4 The mechanism of current rectification in CNTPs between two solutions. (a) Solutions of the same pH: applied voltage and passing of current weakly affects CNTP conductance, showing no rectification. (b) Voltage applied in the forward direction from high to low pH: local pH raised at the high pH end results in a minor increase in CNTP conductance, no current blockage. (c) Voltage applied in the backward direction from low to high pH: local pH drops at high pH end results in a major drop in CNTP conductance, blocking the current. Large red arrows indicate the current direction. Thin arrows next to CNTP mouths indicate ion diffusion, resulting in concentration polarization and a change in local pH. The star indicates local pH controlling CNTP conductivity.

pH 7.5. Salt ions, K⁺ and Cl⁻, have much higher concentrations and are unlikely to produce such an effect. Relevant salt concentrations substituted to eqn (8) yield limiting transfer rates equivalent to currents of the order tens to thousands of picoamperes or molar flow rates 10^{-17} to 10^{-15} mol per s per CNTP (see the ESI†). As these are far larger than the measured currents and permeation rates shown in Fig. 2, the access resistance for these ions should have no effect on the measured transport characteristics of CNTPs.

Conclusions

We have demonstrated that most experimental data on ion transport in narrow (6,6) CNTPs, including both diffusion or electrical measurements, may be rationalized using the pre-

sented molecular model, as an alternative to the commonly considered continuum-like models. The model treats ion partitioning in the mean-field manner considering the uptake of free ions, subject to electroneutrality, to which ion pairing is added to better account for ion-specific effects, with all relevant thermodynamic quantities computed ab initio. We note that, despite the fact that experimental data and their pH and salt concentration dependence strongly suggest a high affinity of (6,6) CNTPs towards hydroxide, the computed transfer energies for single ions do not indicate any such preference. However, computations for ion pairs do reveal a strong affinity to hydroxide, as the exceptionally favorable transfer energy for the KOH pair. In experiments with KCl solutions, this makes K and OH ions dominant species within CNTPs under neutral conditions, which change to K+ and Cl- under acidic conditions. We conclude that the ion transport is apparently controlled by free ions, coexisting with more abundant, but less mobile ion pairs. This also makes hydroxide ions the main charge carrier species in conductance experiments, in contrast to the views in the literature considering potassium as the main charge carrier. The model successfully explains most observed effects of the salt concentration and pH on the conductivity and anion and alkalinity permeation in stop-flow experiments, current rectification, and measured activation energies, as well as molecular mechanisms behind ion transfer and conductance in narrow CNTPs. The only significant discrepancy is found for ion transfer energies fitted to the conductivity data, which yields values lower and, as a result, ion permeability higher than model predictions. Presumably, this may be related to the ion-ion interactions that may reduce the transfer energy for anions and maybe clarified, as more data become available. The proposed modeling approach may be extended to other subnanometer nanochannels and help design next-generation desalination and osmotic energy harvesting materials and devices.

Methods

Computational details

The transfer of H₂O and ions (H⁺, OH⁻, K⁺, and Cl⁻) was computed for the metallic (5,5) and (6,6) nanotubes of diameters 0.68 and 0.80 nm, respectively. For both types, the CNTP fragments used in computations were 1.72 nm long. Thus, the (6,6) tube had seven elementary cells, each containing 24 carbon atoms and total 168 carbon atoms, with dangling bonds at the rims terminated with hydrogen atoms. The species of interest (an ion or a water molecule) was placed in the center of the CNTP and surrounded by four water molecules, two on each side, for the (5,5) tube and by six water molecules, three on each side, for (6,6) tube. This was presumed to be sufficient for cancelling out distant water-water interactions, given ions mainly affect the water structure up to the second hydration shell and only marginally the third one. 60,61 The CNTP with its content was embedded in a dielectric continuum of a dielectric constant ε , viewed as a parameter. For evaluating the thermodynamics of hydration in bulk water, the species of interest was

Paper

surrounded by 6 water molecules, forming a finite cluster embedded in a polarizable continuum of dielectric constant 78.36. Our earlier estimates showed that the use of larger clusters leads to only a marginal improvement, for instance, the difference in ion hydration between 6- and 7-molecule clusters was less than 2 kJ mol^{-1} .⁴⁷ The published data were used to set up the initial cluster geometries for hydrated H_2O , $^{62-64}$ H^+ , 65 OH^- , 65,66 K^+ (ref. 67) and Cl^- . 68,69 To benchmark the computations for interactions of water and ions with aromatic CNT walls, the energies of H_2O and K^+ binding to benzene were computed and compared with experimental values.

The geometries of all structures and thermodynamic properties were calculated *ab initio* using Gaussian 09 Rev. B.01.⁷⁰ The computations employed the combination of the wB97X-D functional⁷¹ including Grimme's D2 dispersion correction⁷² and the 6-31G(d,p) basis set, which was found to yield the best agreement with experimental data on hydration in water. The optimization of structures within CNTP was performed starting from several initial geometries; thereafter, the optimized structure with minimal total electronic energy (E) was selected for further analysis. The IEFPCM polarizable continuum model⁷³ was used to simulate dielectric continua. Zero-point correction energy was computed to convert electronic energies E to enthalpies (H). This correction did not include the vibrational frequency scaling factor, as the associated error at the chosen level of theory was under 1 kJ mol⁻¹ and less than typical errors of ab initio computations.74 Basis set superposition error (BSSE) was estimated using the Boys and Bernardi method⁷⁵ in water/ion clusters and in CNTPs. Apart from electronic energy, the required thermodynamic quantities, i.e., H, excess Gibbs energies (G^{ex}) , and excess entropies (S^{ex}) , included only the vibrational contributions computed using Gaussian, while rotational and translation contributions were discarded, as they consider the corresponding motions of the cluster as a whole and are irrelevant for deriving thermodynamics variables for individual molecules or ions. The transition state of the ion pair flip was localized using the Berny algorithm. The transition state was identified as that with one imaginary vibration frequency. The pair flip barrier was calculated as the difference between the transition and ground (pair aligned with the main CNTP axis) states. Ultimately, the thermodynamic quantities for the transfer of a species from bulk water to water-filled CNTPs, ΔX [ion], were computed using the following relation^{4/2}

$$\Delta X[\text{ion}] = X[\text{CNTP}(\text{H}_2\text{O})_m \text{ion}] + X[(\text{H}_2\text{O})_n] - X[\text{CNTP}(\text{H}_2\text{O})_m] - X[\text{ion}(\text{H}_2\text{O})_n].$$
(9)

The analogous expression for transfer of a cation C^+ and an anion A^- from bulk solution and formation of an ion pair C^+A^- within CNTP was as follows

$$\begin{split} \Delta X[\mathrm{C^+A^-}] = & X[\mathrm{CNTP}(\mathrm{H_2O})_m\mathrm{C^+}] + 2X[(\mathrm{H_2O})_6)] \\ & - X[\mathrm{CNTP}(\mathrm{H_2O})_m] - X[(\mathrm{H_2O})_6\mathrm{C^+}] \\ & - X[(\mathrm{H_2O})_6\mathrm{A^-}]. \end{split} \tag{10}$$

Fig. S1 in the ESI† schematically illustrates transfer processes defined by eqn (9) and (10). Note that different

hydration of cations (K^+ , H^+) and anions (Cl^- , OH^-) resulted in a different arrangement of three adjacent water molecules, resembling zigzag and triple-bonded structures of water, as shown in Fig. 1a and b, respectively. In turn, this could affect the terminal ("surface") energy of the corresponding ion-water and ion pair-water clusters within CNTPs. To ensure this energy is cancelled in the above equations, the energy $X[CNTP(H_2O)_m]$ corresponded to the arrangement resembling the one adjacent to the ion involved or the average of the two arrangements for the ion pairs.

Benchmarking ab initio computations

The transfer quantities critically depend on the reference values for hydration in water. We then first benchmarked computational procedures versus experimental bulk hydration quantities. Fig. S2 in the ESI† demonstrates a good agreement between the computed and experimental values. The deviations for hydration enthalpies H are 3 to 7% of the absolute values. Similar errors were obtained for excess Gibbs energies ΔG^{ex} , but for much smaller entropic terms $T\Delta S^{\text{ex}} = \Delta H - \Delta G^{\text{ex}}$, the deviations were larger, 1% for the water molecule and K⁺, 10% for Cl⁻, and ca. 30% for H⁺ and OH⁻. These errors were considered acceptable, as they may also similarly bias the energies in the bulk and within CNTPs and thus partly cancel out in transfer energies. Besides, the magnitude and sign of deviations, positive for cations and negative for anions, are highly unlikely to affect the physical picture developed here. The present values also agree within a few kJ mol-1 with computations using a higher level of theory ^{62,65,67} and computations using the conductor-like screening model. 76,77

As another benchmarking, most pertinent to interactions with the inner walls of CNTs, we computed the enthalpies of interactions of H_2O and K^+ with benzene, for which both experimental data^{78–80} and computations^{80–84} were reported. Comparison with most accurate data,^{79,80} presented in Fig. S2 in the ESI,† shows deviations under 4 kJ mol⁻¹ of the computed enthalpy for H_2O and 1 kJ mol⁻¹ for K^+ , within typical errors of *ab initio* computations. Our calculations also indicate a negligible interaction of benzene with Cl^- with enthalpy close to zero, in agreement with other reports.^{85,86} The agreement was significantly poorer when no dispersion correction was used. This and the above results indicate that the selected level of theory (wB97X-D/6-31G(d,p)) with dispersion correction was adequate for the present study, given the problem of accurately predicting hydration and solvation energies *ab initio* still has many issues.⁸⁷

Conflicts of interest

There are no conflicts to declare.

Acknowledgements

The financial support from a joint grant 2016627 from the United States-Israel Binational Science Foundation (Israel) and

the National Science Foundation (USA) is acknowledged. The authors thank Aleksandr Noy and Meni Wanunu for discussion and many valuable suggestions.

Notes and references

- 1 A. Mark, Science and technology for water purification in the coming decades, Nature, 2008, 452, 20.
- 2 J. R. Werber, A. Deshmukh and M. Elimelech, The critical need for increased selectivity, not increased water permeability, for desalination membranes, Environ. Sci. Technol. Lett., 2016, 3, 112-120.
- 3 P. Agre, L. S. King, M. Yasui, W. B. Guggino, O. P. Ottersen, Y. Fujiyoshi, A. Engel and S. Nielsen, Aquaporin water channels-from atomic structure to clinical medicine, J. Physiol., 2002, 542, 3-16.
- 4 P. R. Kidambi, D. Jang, J.-C. Idrobo, M. S. Boutilier, L. Wang, J. Kong and R. Karnik, Nanoporous atomically thin graphene membranes for desalting and dialysis applications, J. Adv. Mater., 2017, 29, 1700277.
- 5 D. Jang, J.-C. Idrobo, T. Laoui and R. Karnik, Water and solute transport governed by tunable pore size distributions in nanoporous graphene membranes, ACS Nano, 2017, 11, 10042-10052.
- 6 L. Wang, C. M. Williams, M. S. H. Boutilier, P. R. Kidambi and R. Karnik, Single-layer graphene membranes withstand ultrahigh applied pressure, Nano Lett., 2017, 17, 3081-3088.
- 7 P. R. Kidambi, R. A. Terry, L. Wang, M. S. Boutilier, D. Jang, J. Kong and R. Karnik, Assessment and control of the impermeability of graphene for atomically thin membranes and barriers, Nanoscale, 2017, 9, 8496-8507.
- 8 B. J. Hinds, N. Chopra, T. Rantell, R. Andrews, V. Gavalas and L. G. Bachas, Aligned multiwalled carbon nanotube membranes, Science, 2004, 303, 62-65.
- 9 J. K. Holt, H. G. Park, Y. Wang, M. Stadermann, A. B. Artyukhin, C. P. Grigoropoulos, A. Noy and O. Bakajin, Fast mass transport through sub-2-nanometer carbon nanotubes, Science, 2006, 312, 1034-1037.
- 10 J. K. Holt, A. Noy, T. Huser, D. Eaglesham and O. Bakajin, Fabrication of a carbon nanotube-embedded silicon nitride membrane for studies of nanometer-scale mass transport, Nano Lett., 2004, 4, 2245-2250.
- 11 J. R. Werber, C. O. Osuji and M. Elimelech, Materials for next-generation desalination and water purification membranes, Nat. Rev. Mater., 2016, 1, 1-15.
- 12 X. Lu and M. Elimelech, Fabrication of desalination membranes by interfacial polymerization: history, current efforts, and future directions, Chem. Soc. Rev., 2021, 50(11), 6290-6307.
- 13 Y. Li, Z. Li, F. Aydin, J. Quan, X. Chen, Y.-C. Yao, C. Zhan, Y. Chen, T. A. Pham and A. Noy, Water-ion permselectivity of narrow-diameter carbon nanotubes, Sci. Adv., 2020, 6, eaba9966.

- 14 V. Freger, Selectivity and polarization in water channel membranes: lessons learned from polymeric membranes and CNTs, Faraday Discuss., 2018, 209, 371-388.
- 15 H. Amiri, K. L. Shepard, C. R. Nuckolls and R. Hernández Sánchez, Single-walled carbon nanotubes: mimics of biological ion channels, Nano Lett., 2017, 17, 1204-1211.
- 16 B. Corry, Designing carbon nanotube membranes for efficient water desalination, J. Phys. Chem. B, 2008, 112, 1427-1434.
- 17 C. Song and B. Corry, Intrinsic ion selectivity of narrow hydrophobic pores, *J. Phys. Chem. B*, 2009, **113**, 7642–7649.
- 18 G. Hummer, J. C. Rasaiah and J. P. Noworyta, Water conduction through the hydrophobic channel of a carbon nanotube, Nature, 2001, 414, 188-190.
- 19 A. Striolo, The mechanism of water diffusion in narrow carbon nanotubes, Nano Lett., 2006, 6, 633-639.
- 20 C. Y. Won, S. Joseph and N. Aluru, Effect of quantum partial charges on the structure and dynamics of water in single-walled carbon nanotubes, J. Chem. Phys., 2006, 125, 114701.
- 21 V. V. Chaban, V. V. Prezhdo and O. V. Prezhdo, Confinement by carbon nanotubes drastically alters the boiling and critical behavior of water droplets, ACS Nano, 2012, 6, 2766-2773.
- 22 K. Falk, F. Sedlmeier, L. Joly, R. R. Netz and L. Bocquet, Molecular origin of fast water transport in carbon nanotube membranes: superlubricity versus curvature dependent friction, Nano Lett., 2010, 10, 4067-4073.
- 23 L. Liu and G. Patey, Simulated conduction rates of water through a (6, 6) carbon nanotube strongly depend on bulk properties of the model employed, J. Chem. Phys., 2016, 144, 184502.
- 24 O. N. Samoylova, E. I. Calixte and K. L. Shuford, Molecular dynamics simulations of ion transport in carbon nanotube channels, J. Phys. Chem. C, 2015, 119, 1659-1666.
- 25 R. H. Tunuguntla, R. Y. Henley, Y.-C. Yao, T. A. Pham, M. Wanunu and A. Noy, Enhanced water permeability and tunable ion selectivity in subnanometer carbon nanotube porins, Science, 2017, 357, 792-796.
- 26 R. H. Tunuguntla, F. I. Allen, K. Kim, A. Belliveau and A. Noy, Ultrafast proton transport in sub-1 nm diameter carbon nanotube porins, Nat. Nanotechnol., 2016, 11, 639-644.
- 27 E. Secchi, A. Niguès, L. Jubin, A. Siria and L. Bocquet, Scaling behavior for ionic transport and its fluctuations in individual carbon nanotubes, Phys. Rev. Lett., 2016, 116, 154501.
- 28 M. Majumder, N. Chopra, R. Andrews and B. J. Hinds, Enhanced flow in carbon nanotubes, Nature, 2005, 438, 44-
- 29 S. A. Miller, V. Y. Young and C. R. Martin, Electroosmotic flow in template-prepared carbon nanotube membranes, I. Am. Chem. Soc., 2001, 123, 12335-12342.
- 30 A. Kalra, S. Garde and G. Hummer, Osmotic water transport through carbon nanotube membranes, Proc. Natl. Acad. Sci. U. S. A., 2003, 100, 10175-10180.

31 A. Keerthi, A. Geim, A. Janardanan, A. Rooney, A. Esfandiar, S. Hu, S. Dar, I. Grigorieva, S. Haigh, F. Wang, *et al.*, Ballistic molecular transport through two-dimensional channels, *Nature*, 2018, **558**, 420–424.

Nanoscale

- 32 Y. Hong, J. Zhang, C. Zhu, X. C. Zeng and J. S. Francisco, Water desalination through rim functionalized carbon nanotubes, *J. Mater. Chem. A*, 2019, 7, 3583–3591.
- 33 Y. Hou, M. Wang, X. Chen and X. Hou, Continuous waterwater hydrogen bonding network across the rim of carbon nanotubes facilitating water transport for desalination, *Nano Res.*, 2021, 1–8.
- 34 B. Corry, Water and ion transport through functionalised carbon nanotubes: implications for desalination technology, *Energy Environ. Sci.*, 2011, 4, 751–759.
- 35 P. Biesheuvel and M. Bazant, Analysis of ionic conductance of carbon nanotubes, *Phys. Rev. E*, 2016, **94**, 050601.
- 36 Y. Uematsu, R. R. Netz, L. Bocquet and D. J. Bonthuis, Crossover of the power-law exponent for carbon nanotube conductivity as a function of salinity, *J. Phys. Chem. B*, 2018, 122, 2992–2997.
- 37 N. Kavokine, R. R. Netz and L. Bocquet, Fluids at the nanoscale: From continuum to subcontinuum transport, *Annu. Rev. Fluid Mech.*, 2021, 53, 377–410.
- 38 Y. Noh and N. R. Aluru, Ion transport in electrically imperfect nanopores, *ACS Nano*, 2020, 14, 10518–10526.
- 39 Z. Sarkadi, D. Fertig, Z. Ható, M. Valiskó and D. Boda, From nanotubes to nanoholes: Scaling of selectivity in uniformly charged nanopores through the Dukhin number for 1: 1 electrolytes, *J. Chem. Phys.*, 2021, 154, 154704.
- 40 Y.-C. Yao, A. Taqieddin, M. A. Alibakhshi, M. Wanunu, N. R. Aluru and A. Noy, Strong electroosmotic coupling dominates ion conductance of 1.5 nm diameter carbon nanotube porins, ACS Nano, 2019, 13, 12851–12859.
- 41 M. Manghi, J. Palmeri, K. Yazda, F. Henn and V. Jourdain, Role of charge regulation and flow slip in the ionic conductance of nanopores: An analytical approach, *Phys. Rev. E*, 2018, **98**, 012605.
- 42 X. Gao, Molecular Dynamics Study of Water and Ion Transport in Carbon Nanotubes and Slit Nanochannels, Hong Kong University of Science and Technology, Hong Kong, 2017.
- 43 T. A. Beu, Molecular dynamics simulations of ion transport through carbon nanotubes. I. Influence of geometry, ion specificity, and many-body interactions, *J. Chem. Phys.*, 2010, **132**, 164513.
- 44 T. A. Beu, Molecular dynamics simulations of ion transport through carbon nanotubes. II. Structural effects of the nanotube radius, solute concentration, and applied electric fields, *J. Chem. Phys.*, 2011, 135, 044515.
- 45 A.-E. Ailenei and T. A. Beu, Ion transport through gated carbon nanotubes: molecular dynamics simulations using polarizable water, *J. Mol. Struct.*, 2021, 131022.
- 46 Z. Li, Y. Li, Y.-C. Yao, F. Aydin, C. Zhan, Y. Chen, M. Elimelech, T. A. Pham and A. Noy, Strong Differential Monovalent Anion Selectivity in Narrow Diameter Carbon Nanotube Porins, ACS Nano, 2020, 14, 6269–6275.

- 47 V. Neklyudov and V. Freger, Water and Ion Transfer to Narrow Carbon Nanotubes: Roles of Exterior and Interior, *J. Phys. Chem. Lett.*, 2020, 12, 185–190.
- 48 B. Grosjean, C. Pean, A. Siria, L. Bocquet, R. Vuilleumier and M.-L. Bocquet, Chemisorption of hydroxide on 2D materials from DFT calculations: graphene versus hexagonal boron nitride, *J. Phys. Chem. Lett.*, 2016, 7, 4695–4700.
- 49 O. Beckstein and M. S. Sansom, The influence of geometry, surface character, and flexibility on the permeation of ions and water through biological pores, *Phys. Biol.*, 2004, **1**, 42.
- 50 A. Waghe, J. C. Rasaiah and G. Hummer, Entropy of single-file water in (6, 6) carbon nanotubes, *J. Chem. Phys.*, 2012, 137, 044709.
- 51 K. V. Agrawal, S. Shimizu, L. W. Drahushuk, D. Kilcoyne and M. S. Strano, Observation of extreme phase transition temperatures of water confined inside isolated carbon nanotubes, *Nat. Nanotechnol.*, 2017, 12, 267–273.
- 52 C. Zhan, F. Aydin, E. Schwegler, A. Noy and T. A. Pham, Understanding Cation Selectivity in Carbon Nanopores with Hybrid First-Principles/Continuum Simulations: Implications for Water Desalination and Separation Technologies, *ACS Appl. Nano Mater.*, 2020, 3, 9740–9748.
- 53 J. P. Dilger, S. McLaughlin, T. J. McIntosh and S. A. Simon, The dielectric constant of phospholipid bilayers and the permeability of membranes to ions, *Science*, 1979, **206**, 1196–1198.
- 54 F. Aydin, A. Moradzadeh, C. L. Bilodeau, E. Y. Lau, E. Schwegler, N. R. Aluru and T. A. Pham, Ion Solvation and Transport in Narrow Carbon Nanotubes: Effects of Polarizability, Cation-π Interaction, and Confinement, *J. Chem. Theory Comput.*, 2021, 17, 1596–1605.
- 55 A. Levy, J. P. de Souza and M. Z. Bazant, Breakdown of electroneutrality in nanopores, *J. Colloid Interface Sci.*, 2020, 579, 162–176.
- 56 S. H. Lee and J. C. Rasaiah, Proton transfer and the diffusion of H+ and OH- ions along water wires, *J. Chem. Phys.*, 2013, **139**, 124507.
- 57 C. Dellago, M. M. Naor and G. Hummer, Proton transport through water-filled carbon nanotubes, *Phys. Rev. Lett.*, 2003, **90**, 105902.
- 58 B. Grosjean, M.-L. Bocquet and R. Vuilleumier, Versatile electrification of two-dimensional nanomaterials in water, *Nat. Commun.*, 2019, **10**, 1–8.
- 59 V. Freger, Ion partitioning and permeation in charged low-T* membranes, *Adv. Colloid Interface Sci.*, 2020, 277, 102107.
- 60 P. Schienbein, G. Schwaab, H. Forbert, M. Havenith and D. Marx, Correlations in the solute–solvent dynamics reach beyond the first hydration shell of ions, *J. Phys. Chem. Lett.*, 2017, 8, 2373–2380.
- 61 V. Balos, S. Imoto, R. R. Netz, M. Bonn, D. J. Bonthuis, Y. Nagata and J. Hunger, Macroscopic conductivity of aqueous electrolyte solutions scales with ultrafast microscopic ion motions, *Nat. Commun.*, 2020, 11, 1–8.
- 62 M. Gillan, D. Alfe and A. Michaelides, *J. Chem. Phys.*, 2016, 144, 130901.

- 63 F. Li, L. Wang, J. Zhao, J. R.-H. Xie, K. E. Riley and Z. Chen, What is the best density functional to describe water clusters: Evaluation of widely used density functionals with various basis sets for $(H_2O)_n$ (n = 1-10), Theor. Chem. Acc., 2011, 130, 341-352.
- 64 B. Temelso, K. A. Archer and G. C. Shields, Benchmark structures and binding energies of small water clusters with anharmonicity corrections, J. Phys. Chem. A, 2011, 115, 12034-12046.
- 65 J. Mejias and S. Lago, Calculation of the absolute hydration enthalpy and free energy of H+ and OH-, J. Chem. Phys., 2000, 113, 7306-7316.
- 66 M. Śmiechowski and J. Stangret, Hydroxide ion hydration in aqueous solutions, J. Phys. Chem. A, 2007, 111, 2889-2897.
- 67 J. Srinivasa Rao, T. Dinadayalane, J. Leszczynski and G. Narahari Sastry, Comprehensive Study on the Solvation of Mono-and Divalent Metal Cations: Li+, Na+, K+, Be2+, Mg2+ and Ca, J. Phys. Chem. A, 2008, 112, 12944-12953.
- 68 D. J. Tobias, P. Jungwirth and M. Parrinello, Surface solvation of halogen anions in water clusters: An ab initio molecular dynamics study of the Cl-(H 2 O) 6 complex, J. Chem. Phys., 2001, 114, 7036-7044.
- 69 P. Bajaj, M. Riera, J. K. Lin, Y. E. Mendoza Montijo, J. Gazca and F. Paesani, Halide Ion Microhydration: Structure, Energetics, and Spectroscopy of Small Halide-Water Clusters, J. Phys. Chem. A, 2019, 123, 2843-2852.
- 70 M. J. Frisch, et al., Gaussian 09 Revision B.01, 2009.
- 71 J.-D. Chai and M. Head-Gordon, Long-range corrected hybrid density functionals with damped atom-atom dispersion corrections, Phys. Chem. Chem. Phys., 2008, 10, 6615-6620.
- 72 S. Grimme, J. Antony, S. Ehrlich and H. Krieg, A consistent and accurate ab initio parametrization of density functional dispersion correction (DFT-D) for the 94 elements H-Pu, J. Chem. Phys., 2010, 132, 154104.
- 73 J. Tomasi, B. Mennucci and R. Cammi, Quantum mechanical continuum solvation models, Chem. Rev., 2005, 105, 2999-3094.
- 74 M. L. Laury, M. J. Carlson and A. K. Wilson, Vibrational frequency scale factors for density functional theory and the polarization consistent basis sets, J. Comput. Chem., 2012, 33, 2380-2387.
- 75 S. F. Boys and F. Bernardi, The calculation of small molecular interactions by the differences of separate total energies. Some procedures with reduced errors, Mol. Phys., 1970, 19, 553-566.

- 76 V. Barone and M. Cossi, Quantum calculation of molecular energies and energy gradients in solution by a conductor solvent model, J. Phys. Chem. A, 1998, 102, 1995-2001.
- 77 M. Cossi, G. Scalmani, N. Rega and V. Barone, Energies, gradients, and harmonic frequencies for molecules in solution by the C-PCM solvation model, I. Comput. Chem., 2003, 24, 669.
- 78 Y. Marcus and A. Ben Naim, Solvation, dynamics of nonionic solutes, J. Chem. Phys., 1984, 81, 2016-2027.
- 79 J. C. Amicangelo and P. Armentrout, Absolute binding energies of alkali-metal cation complexes with benzene determined by threshold collision-induced dissociation experiments and ab initio theory, J. Phys. Chem. A, 2000, 104, 11420-11432.
- 80 A. Courty, M. Mons, I. Dimicoli, F. Piuzzi, M.-P. Gaigeot, V. Brenner, P. de Pujo and P. Millié, Quantum Effects in the Threshold Photoionization and Energetics of the Benzene- H2O and Benzene- D2O Complexes: Experiment and Simulation, J. Phys. Chem. A, 1998, 102, 6590-6600.
- 81 A. Ferretti, G. Prampolini and M. d'Ischia, Benchmarking Cation-π Interactions: Assessment of DFT and Moeller-Plesset Second Order Perturbation Theory Calculations with Optimized Basis Sets (MP2mod) for Complexes of Benzene, Phenol and Catechol with Na+, K+, Rb+ and Cs+, I. Phys. Chem. A, 2020, 124, 3445-3459.
- 82 D. Upadhyay and P. Mishra, Binding of benzene with water clusters (H_2O) n, n = 1-6, in the ground and lowest singlet excited states, J. Mol. Struct.: THEOCHEM, 2002, 584, 113-133.
- 83 J. Ma, D. Alfè, A. Michaelides and E. Wang, The waterbenzene interaction: Insight from electronic structure theories, J. Chem. Phys., 2009, 130, 154303.
- 84 P. Schyman and W. L. Jorgensen, Exploring adsorption of water and ions on carbon surfaces using a polarizable force field, J. Phys. Chem. Lett., 2013, 4, 468-474.
- 85 S. E. Wheeler and K. Houk, Are Anion/ π Interactions Actually a Case of Simple Charge- Dipole Interactions?, I. Phys. Chem. A, 2010, 114, 8658-8664.
- 86 X. Lucas, D. Quinonero, A. Frontera and P. M. Deya, Counterintuitive Substituent Effect of the Ethynyl Group in Ion-π Interactions, J. Phys. Chem. A, 2009, 113, 10367-10375.
- 87 L. Vlcek and A. A. Chialvo, Single-ion hydration thermodynamics from clusters to bulk solutions: Recent insights from molecular modeling, Fluid Ph. Equilibria, 2016, 407, 58-75.